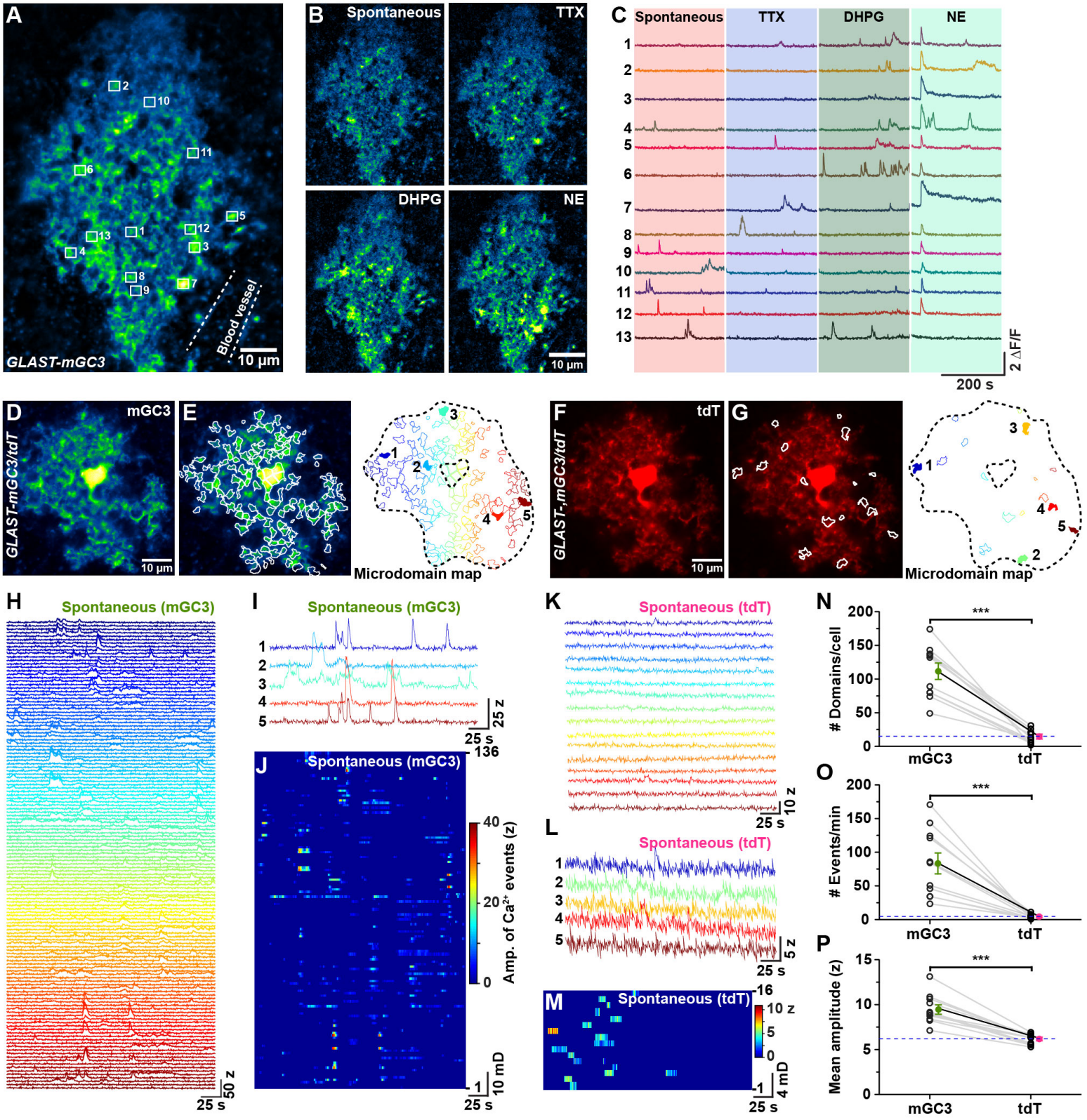

Figure S1, Agarwal et al.

Figure S1: Characteristics of Ca^{2+} transients in astrocytes visualized with mGCaMP3 and tdTomato (related to Figure 2).

(A) Image of one astrocyte from a *GLAST-mGC3* mouse, showing median intensity projection (pseudocolored) from 540 frames in time-series images acquired at 2.1 Hz (260 s). Regions of interests were manually selected for 13 areas exhibiting spontaneous changes in fluorescence.

(B) Images of astrocyte in (A) showing maximum intensity projection (pseudocolored) during baseline (Spontaneous), after treatment with TTX (1 μM), and after exposure to agonists of metabotropic glutamate receptors (DHPG, 20 μM) and adrenergic receptors (norepinephrine, NE, 10 μM). Agonists were applied with 1 μM TTX.

(C) Intensity versus time traces for 14 manually selected microdomains (numbers correspond to boxes in (A), showing characteristics of Ca^{2+} transients in control (Spontaneous), and after treatment with TTX, DHPG (+ TTX) and NE (+ TTX). Note that even neighboring domains (#s 8 & 9, and #s 12 & 13) exhibited distinct Ca^{2+} signals that were temporally uncorrelated.

(D) Image of one astrocyte from a *GLAST-mGC3/tdT* mouse showing median intensity projection (pseudocolored) of mGCaMP3 fluorescence from 540 frames in time-series images acquired at 2.1 Hz (260 s).

(E) Map of 136 spontaneously active microdomains recorded in control overlaid on median intensity projected image in (D) (left). The isolated microdomain map (color coded according to location) detected using the CaSCaDe analysis is shown at right.

(F) Image of astrocyte in (D) from a *GLAST-mGC3/tdT* mouse showing median intensity projection (pseudocolored) of tdT fluorescence from 540 frames in time-series images acquired at 2.1 Hz (260 s).

(G) Map of 16 false positive "microdomains" (left) overlaid on the median intensity projected image of tdT fluorescence (right). The isolated microdomain map (color coded according to location) generated using CaSCaDe analysis is shown at right. This analysis had an error rate estimated from selection of these false positives of 10 % (compare to (E)).

(H) Intensity versus time traces for spontaneous Ca^{2+} signals (mGCaMP3 fluorescence) from all 136 spontaneously active microdomains imaged over a period of 260 s. Traces color coded according to location show in (E).

(I) Intensity versus time traces for spontaneous Ca^{2+} signals (mGCaMP3 fluorescence) from 5 microdomains (corresponding to colors highlighted in (E)).

(J) Raster plot of microdomain activity, color-coded according to fluorescence change (z-score).

(K) Intensity versus time traces showing tdT fluorescence changes from all 16 regions identified over a period of 260 s.

(L) Intensity versus time traces for tdT fluorescence changes detected by CaSCaDe analysis from 5 microdomains. Colors correspond to locations highlighted in (G).

(M) Raster plot of tdT fluorescence changes (z-score) for regions detected using CaSCaDe analysis.

(N-P) Graphs comparing the number of active microdomains (N), event frequency (O) and average event amplitude (P) (z-score) for mGCaMP3 and tdT fluorescence changes detected by CaSCaDe analysis. Data shown as mean ± SEM. N = 11 cells (*GLAST-mGC3/tdT* mice). *** $p < 0.0004$, paired two-tailed Student's t-test.

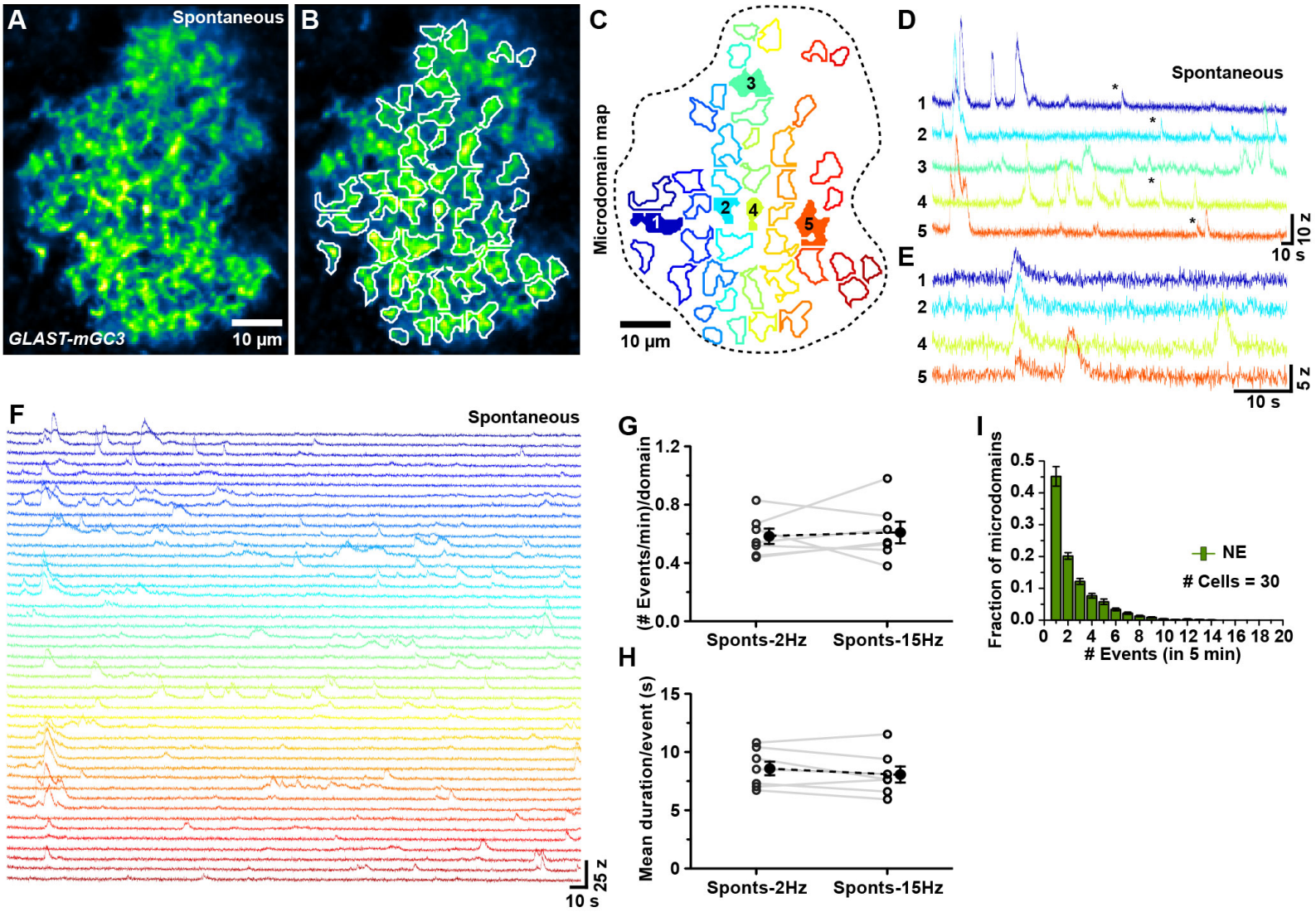

Figure S2, Agarwal et al.

Figure S2: Analysis of microdomain Ca^{2+} transient kinetics using rapid imaging (related to Figure 3).

(A) Image of one astrocyte in an acute brain slice from a *GLAST-mGC3* mouse showing median intensity projection (pseudocolored) of mGCaMP3 fluorescence from 260 s (3900 frames @ 15 Hz).

(B, C) Map of spontaneously active microdomains overlaid on the median intensity projected image (B). Dashed line highlights cell border. The isolated microdomain map (color coded according to location) is shown in (C).

(D, E) Intensity versus time traces showing spontaneous Ca^{2+} signals in five microdomains selected from different locations in the astrocyte (corresponding to colors shown in (C)). Several rapid Ca^{2+} transients (marked with asterisks in (D)) are shown on a faster time scale in (E), illustrating that they occur on a time scale of seconds.

(F) Intensity versus time traces showing mGCaMP3 fluorescence changes from all 45 spontaneously active microdomains imaged over a period of 260 s. Traces are color coded according to location in (C).

(G, H) Graphs comparing frequency of events per domain (G) and average event duration (H) for spontaneous Ca^{2+} transients imaged at 2.1 Hz and 15 Hz. Data shown as mean ± SEM. N = 7 cells from *GLAST-mGC3* mice. ns, not significant, paired two-tailed Student's t-test.

(I) Histogram of the number of Ca^{2+} transients observed per microdomain in NE (+ TTX) (compare to Figure 4P). Data shown as mean ± SEM. N = 30 cells for NE from *GLAST-mGC3* mice.

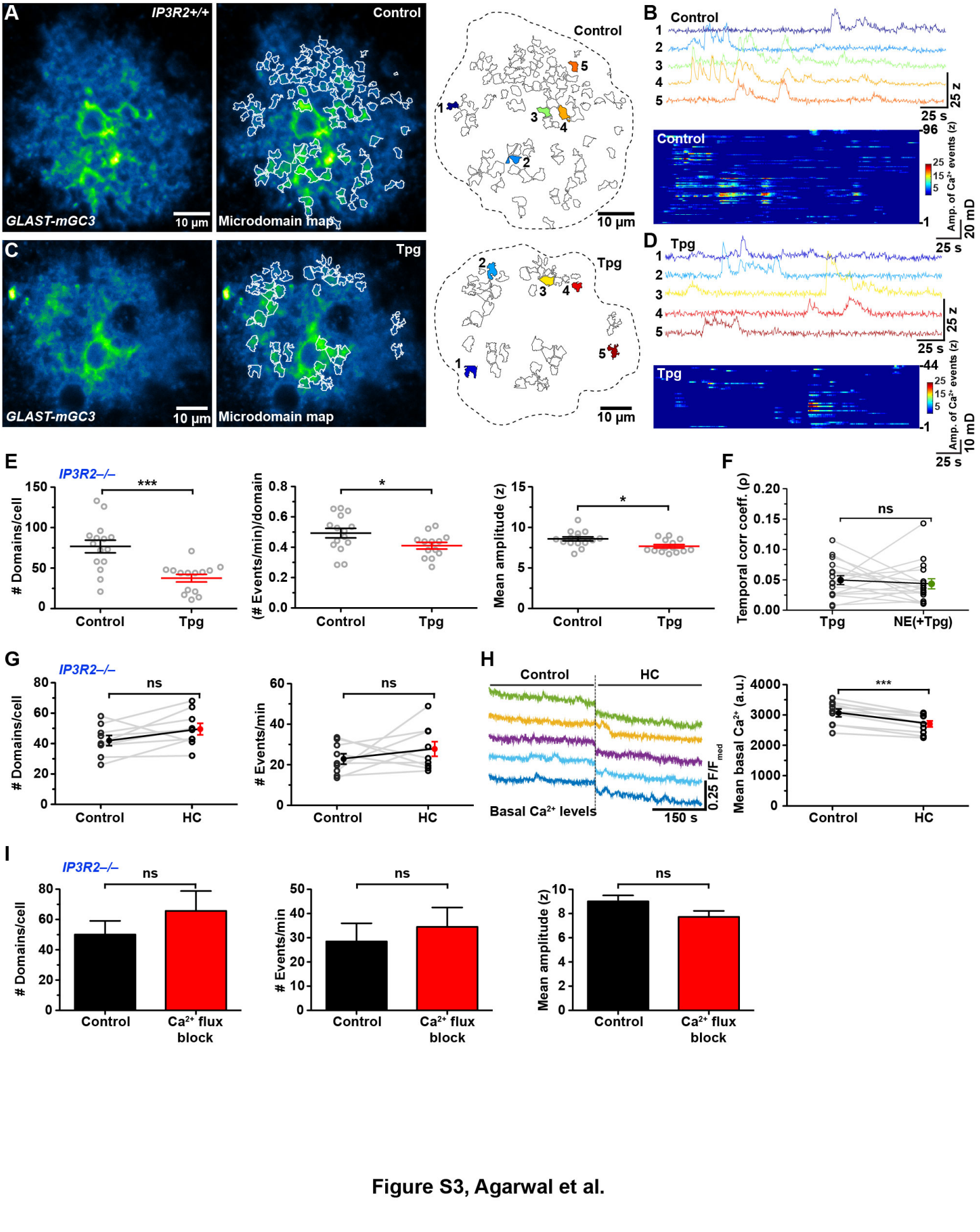

Figure S3, Agarwal et al.

Figure S3: Spontaneous Ca^{2+} transients persist in astrocytes from *IP3R2–/–* mice in the presence of inhibitors of channels and receptors that mediate transmembrane Ca^{2+} fluxes (related to Figure 4).

(A) Image of one astrocyte in an acute brain slice from a *GLAST-mGC3* mouse showing median intensity projection (pseudocolored) of mGCaMP3 fluorescence from 260 s (left). Map of spontaneously active microdomains is overlaid on the median intensity projected image (middle) and shown separately at right.

(B) Intensity versus time traces showing Ca^{2+} transients in five microdomains (colors correspond to locations in (A, right)) (top). Raster plot of Ca^{2+} signals from 96 spontaneously active microdomains imaged over a period of 260 s (bottom).

(C) Image of one astrocyte in an acute brain slice from a *GLAST-mGC3* mouse showing median intensity projection (pseudocolored) of mGCaMP3 fluorescence from 260 s (left) after treatment with thapsigargin (Tpg, 1 μM, 60 minutes). Map of spontaneously active microdomains is overlaid on the median intensity projected image (middle) and shown separately at right. Dashed line highlights cell border.

(D) Intensity versus time traces showing Ca^{2+} transients in five microdomains (colors correspond to locations in (C, right)) (top). Raster plot of Ca^{2+} signals from 44 spontaneously active microdomains imaged over a period of 260 s recorded in Tpg (bottom).

(E) Graphs comparing number of domains/cell (left), frequency of events/domain (middle) and mean amplitude of microdomain Ca^{2+} transients (right) in control and Tpg treated cortical slices. Data shown as mean ± SEM. N = 15 cells for control and 14 cells in Tpg. All recordings from *GLAST-mGC3* mice. *** $p < 0.0002$, * $p < 0.05$, unpaired two-tailed Student's t-test.

(F) Graph comparing temporal correlation between microdomain Ca^{2+} transients during baseline (+Tpg, +TTX) and in NE (+Tpg, +TTX). Note that application of NE in the presence of Tpg failed to synchronize microdomain activity (compare to Figure 3E, F). Data shown as mean ± SEM. N = 17 cells from *GLAST-mGC3* mice. ns, not significant, paired two-tailed Student's t-test.

(G) Graphs comparing number of active microdomains/cell (left) and frequency of microdomain Ca^{2+} transients (right) in control and in the presence of the TRPA1 antagonist, HC030031 (HC, 50 μM, 10 min). All experiments performed in the presence of 1 μM TTX. Data shown as mean ± SEM. N = 9 cells from *GLAST-mGC3;IP3R2–/–* mice. ns, not significant, paired two-tailed Student's t-test.

(H) Intensity versus time traces showing decrease in resting mGCaMP3 fluorescence levels in astrocytes after treatment with HC030031 (HC, 50 μM, 10 min). All experiments performed in 1 μM TTX. Data shown as mean ± SEM. N = 9 cells from *GLAST-mGC3;IP3R2–/–* mice. *** $p = 0.0003$, paired two-tailed Student's t-test.

(I) Histograms comparing number of domains/cell, frequency of events and mean amplitude (z-score) of microdomain Ca^{2+} transients in control and in the presence of antagonists that block Ca^{2+} channels and receptors, including CRAC channels (Synta-66/GSK7975A, 10 μM), ryanodine receptors (dantrolene, 10 μM), voltage dependent Ca^{2+} channels (cadmium chloride, 100 μM), Na/Ca^{2+} exchangers (benzamil, 100 μM and CGP37157, 20 μM) and TRPA1 channels (HC030031, 50 μM). All experiments performed in 1 μM TTX. Slices were treated with antagonists for 60 min at room temperature prior to imaging. Data shown as mean ± SEM. N = 11 cells for control slices and 7 cells from slices treated with antagonists. All experiments performed using tissue from *GLAST-mGC3;IP3R2–/–* mice. ns, not significant, unpaired two-tailed Student's t-test.

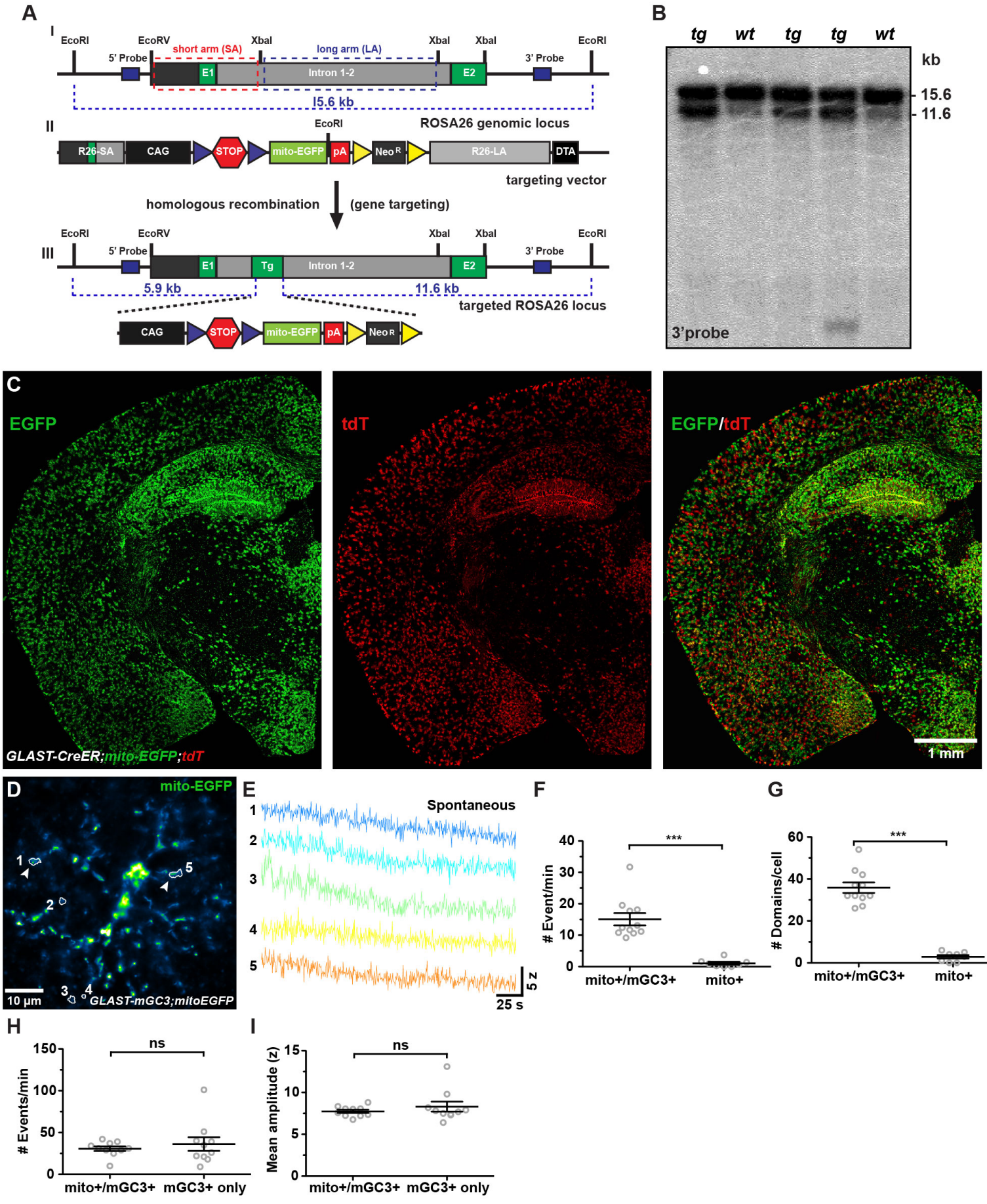

Figure S4, Agarwal et al.

Figure S4: Conditional expression of mitochondrial targeted EGFP in astrocytes (related to Figure 6).

(A) Schematic showing the gene trap strategy used to insert mito-EGFP transgene into the murine Rosa26 gene. (I) Genomic structure of the mouse Rosa26 allele. The locus comprises two exons (E1 and E2; green boxes). (II) Structure of mito-EGFP targeting vector. The construct harbors 5' (R26-SA) and 3' (R26-LA) homology arms from Rosa26, the CMV enhancer chicken β-actin hybrid (CAG) promoter (black box), loxP flanked 3x SV40-polyA sequence ("STOPPER" blue triangles and red hexagon), the mito-EGFP cDNA (light green box) and bovine growth hormone polyA sequence (red box). (III) Rosa26 allele after homologous recombination in murine ES cells.

(B) Southern blot analysis of genomic DNA derived from ES cells targeted with mito-EGFP, using 3' probe (top, indicated in Blue in A I) reveals one product (15.6 kb) in wildtype (wt), two products (11.6 kb, 15.6 kb) in heterozygotes (tg).

(C) Coronal hemi-section of brain from a *GLAST-CreER;Rosa26-lsl-mito-EGFP;Rosa26-lsl-tdTomato* (*GLAST-mito-EGFP/tdT*) triple transgenic mouse immunostained for mito-EGFP (anti-EGFP, left) and tdT (anti-mCheery, middle), showing widespread expression of mito-EGFP in cortical and hippocampal astrocytes. Overlay is shown at right.

(D) Image of mito-EGFP fluorescence in one cortical astrocyte from a *GLAST-mGC3/mitoEGFP* mouse showing median intensity projection of time-series image stack (pseudocolored) for 260 s of imaging. Map of active regions detected by CaSCaDe analysis is overlaid on image.

(E) Intensity versus time traces showing spontaneous activity detected in five microdomains by CaSCaDe analysis (numbered according to locations in D).

(F, G) Graphs comparing the frequency of microdomain Ca^{2+} transients (F) and number of domains/cell (G) in astrocytes co-expressing mGCaMP3 and mito-EGFP (mito+/mGC3+), to astrocytes solely expressing mito-EGFP (mito+). Note the low false positive rate in mito+. Data shown as mean ± SEM. N = 11 mito+/mGC3+ cells and 8 mito+ cells from *GLAST-mGC3/mito-EGFP* mice. *** p = 0.0003, two tailed Mann Whitney test (F) and *** p < 0.0001, unpaired two-tailed Student's t-test (G).

(H, I) Graphs comparing frequency (H) and mean amplitude of microdomain Ca^{2+} transients (I) in astrocytes co-expressing mGCaMP3 and mito-EGFP (mito+/mGC3+), to astrocytes that only expressed mGCaMP3 (mGC3+ only). Data shown as mean ± SEM (n = 10 cells, *GLAST-mGC3/mito-EGFP* mice). ns, not significant, two-tailed Wilcoxon matched pairs test (H), and paired two-tailed Student's t-test (I).

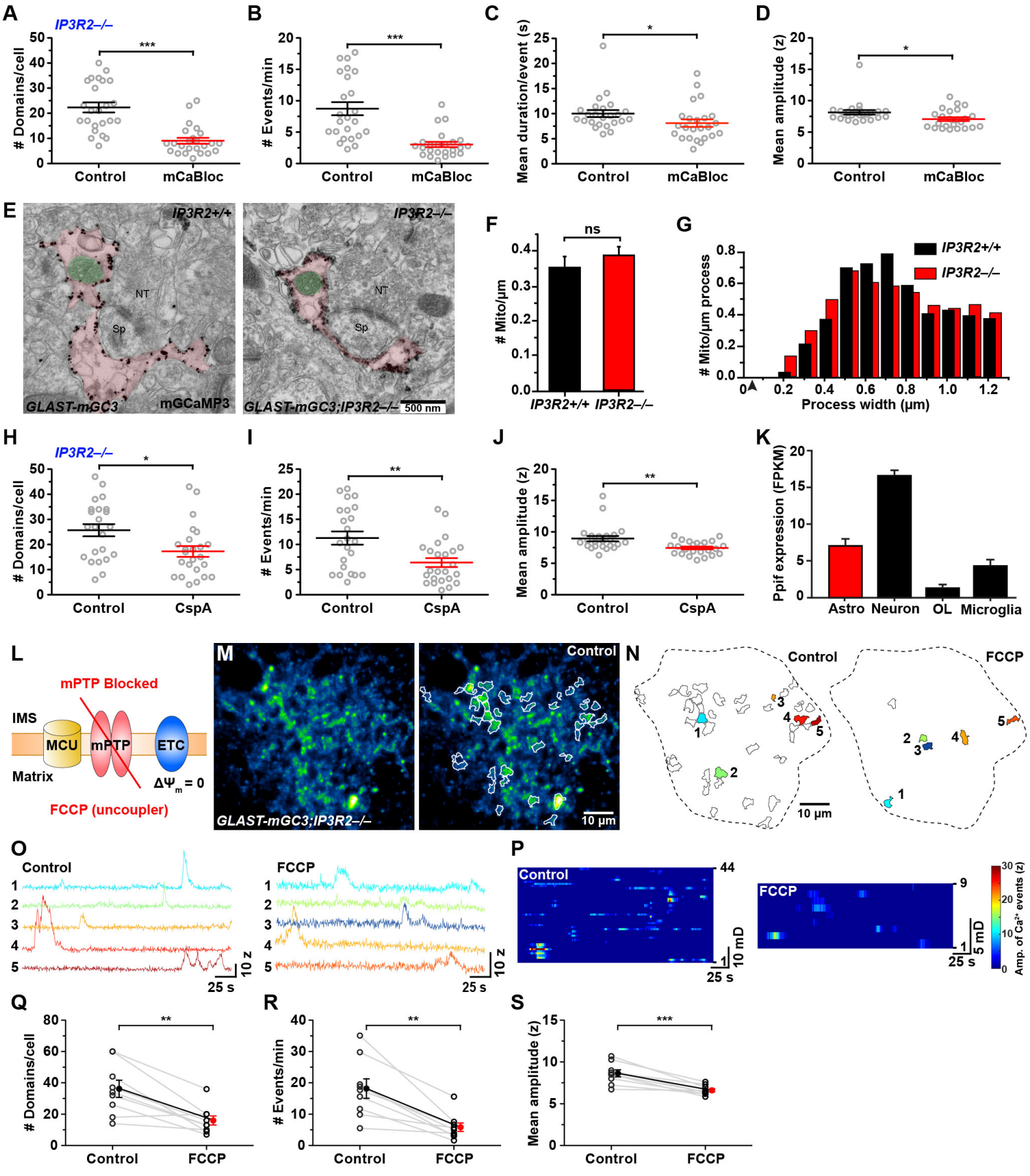

Figure S5, Agarwal et al.

Figure S5: Modulation of mPTP activity alters spontaneous microdomain Ca^{2+} transients in astrocytes lacking IP3R2 (related to Figure 7).

(A-D) Graphs comparing number of domains/cell (A), frequency of events (B), mean duration of events (C) and mean amplitude of microdomain Ca^{2+} transients (z-score, D) in control and in the presence of antagonists that block mitochondrial Ca^{2+} fluxes (mCaBloc), including the mitochondrial uniporter (MCU, KB-R7943 mesylate, 20 µM), mPTP (cyclosporin A, 20 µM) and the Na/Ca^{2+} exchanger (CGP37157, 20 µM). All experiments performed in 1 µM TTX. Slices were treated with a mCaBloc for 60 min prior to imaging. Data shown as mean ± SEM. N = 24 cells for each condition. All cortical slices derived from *GLAST-mGC3;IP3R2–/–* mice. *** $p < 0.0001$, * $p = 0.026$, unpaired two-tailed Student's t-test.

(E) Electron micrographs showing silver intensified immunogold labeling for mGCaMP3 (anti-EGFP). The locations of mitochondria (colored green) in astrocyte processes (colored red) are highlighted in control *IP3R2+/+* (*GLAST-mGC3*) and *IP3R2–/–* (*GLAST-mGC3,IP3R2–/–*) mice.

(F, G) Histogram comparing the number of mitochondria/µm in astrocyte processes of control *GLAST-mGC3* (*IP3R2+/+*) and *GLAST-mGC3,IP3R2–/–* (*IP_3R2–/–*, red) mice (F). Histogram comparing the distribution of mitochondria in processes of astrocytes in *IP3R2+/+* (black bars) and *IP_3R2–/–* (red bars) mice (G). ns: not significant, $p > 0.05$ unpaired two-tailed Student's t-test.

(H – J) Graphs comparing number of domains/cell (H), frequency of events (I), and mean amplitude of microdomain Ca^{2+} transients (z-score, J) in astrocytes from control and in the presence of cyclosporin A (CspA, 20 µM). All experiments performed in 1 µM TTX. Slices were with CspA for 60 min prior to imaging. Data shown as mean ± SEM. N = 23 cells for control slices and 24 cells for CspA. All cortical slices derived from *GLAST-mGC3,IP3R2–/–* mice. ** $p = 0.003$, * $p = 0.012$, unpaired two-tailed Student's t-test.

(K) Expression of cyclophilin D (Ppif mRNA) by neurons and glial cells. Data from (Zhang et al., 2014). http://web.stanford.edu/group/barres_lab/cgi-bin/igv_cgi_2.py?lname=ppif Note much lower level of cyclophilin D mRNA in astrocytes (red) compared to neurons (black).

(L) Schematic showing configuration of membrane permeability transition pore (mPTP), mitochondrial Ca^{2+} uniporter (MCU) and the electron transport chain (ETC). The action of ETC generates a proton gradient ($\Delta\Psi$) across inner mitochondrial membrane (IMM) and matrix. FCCP (5 µM) inhibits opening of mPTP by dissipating the proton gradient ($\Delta\Psi$), preventing Ca^{2+} efflux from the mitochondrial matrix into the cytosol.

(M) Image of one astrocyte in an acute brain slice from a *GLAST-mGC3;IP3R2–/–* mouse showing median intensity projection (pseudocolored) of mGCaMP3 fluorescence from 260 s (left). Map of spontaneously active microdomains is overlaid on the median intensity projected image (middle) and show separately at right.

(N) Maps showing location of spontaneous active microdomains in control (44 domains, left) and in FCCP (9 domains, right) from an astrocyte in a *GLAST-mGC3;IP3R2–/–* mouse that occurred during 260 s of imaging. Dashed line highlights cell border.

(O) Intensity versus time traces showing Ca^{2+} transients in 5 microdomains in untreated controls (left) (colors correspond to locations in N, left) and in slices exposed to FCCP for 10 min (right) (colors correspond to locations in N, right).

(P) Raster plots of Ca^{2+} signals from 44 active microdomains in control (left) and nine in FCCP treated slices (right) imaged over a period of 260 s.

(Q – S) Graphs comparing the number of domains/cell (Q), frequency of events (R) and mean amplitude of microdomain Ca^{2+} transients (z-score, S) in astrocytes from control and FCCP (5 µM) treated slices. All experiments performed in 1 µM TTX. Data shown as mean ± SEM. N = 9 cells for each condition. All cortical slices derived from *GLAST-mGC3;IP3R2–/–* mice. *** $p < 0.0004$, ** $p < 0.004$, paired two-tailed Student's t-test.

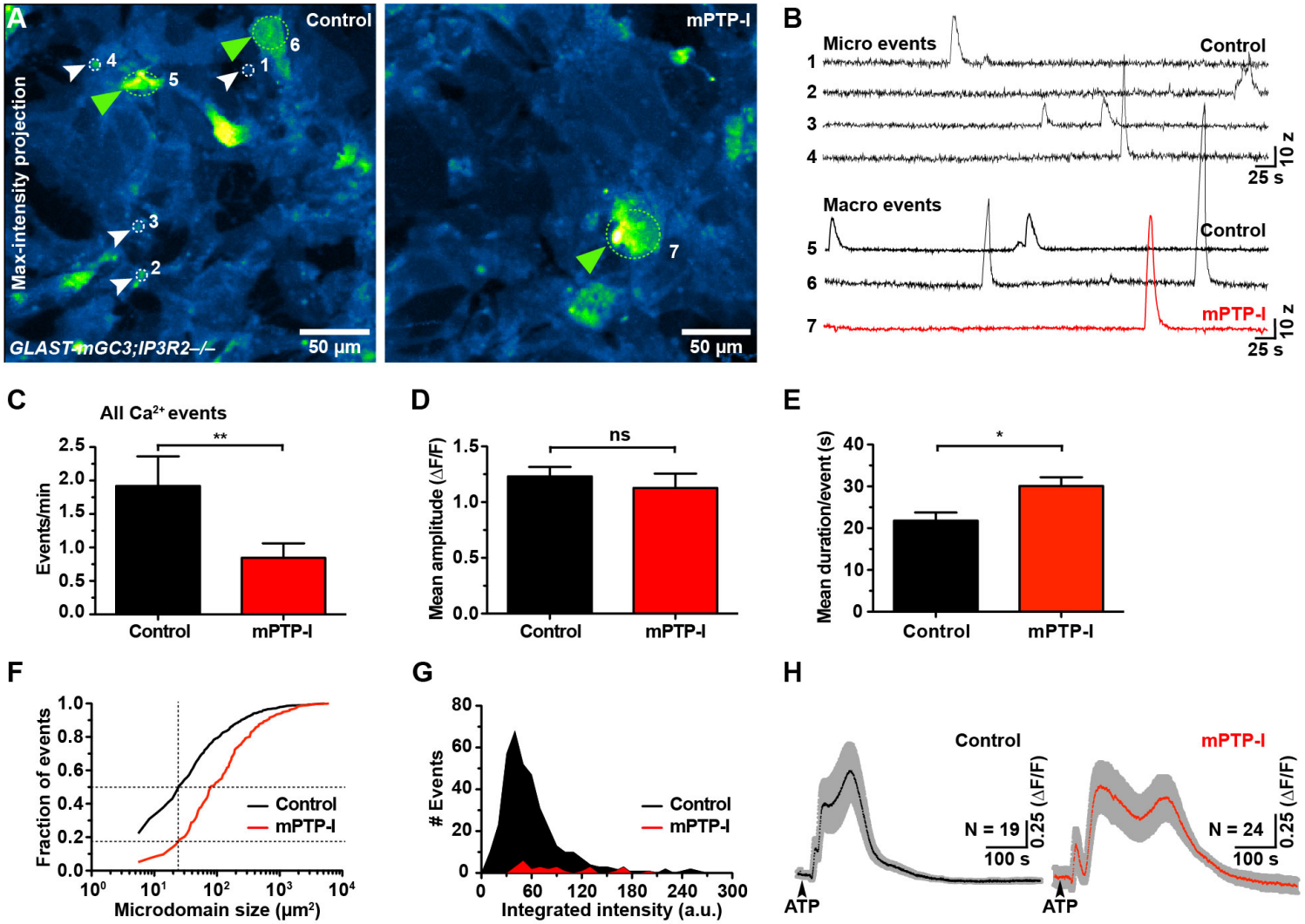

Figure S6, Agarwal et al.

Figure S6: mPTP regulates microdomain Ca^{2+} transients in cultured cortical astrocytes derived from *IP3R2–/–* mice (related to Figure 7)

(A) Image of cortical astrocytes in culture from *GLAST-mGC3;IP3R2–/–* mice, Control (left) and cells after treatment with mPTP inhibitors (mPTP-I, 60 minutes) (right), showing maximum intensity projection (pseudocolored) of mGCaMP3 fluorescence over 540 s.

(B) Intensity versus time traces from four near-membrane restricted microdomains events (micro events) in untreated astrocytes (Control, top) and larger spreading events (macro events) from untreated (Control, black, bottom) and mPTP-I treated (mPTP-I, red, bottom) astrocytes showing characteristics of *in vitro* baseline Ca^{2+} signals.

(C – E) Graphs comparing the frequency (C), mean amplitude (D) and mean duration (E) of all Ca^{2+} transients in untreated (Control, black) and mPTP inhibitor-treated (mPTP-I, red) astrocytes. Data shown as mean ± SEM. Number of coverslips (N) = 10 for untreated (Control) and N = 11 for mPTP-I treated (mPTP-I) conditions. ** $p < 0.007$ (Mann-Whitney test), ns: not significant and * $p < 0.01$, unpaired two-tailed Student's t-test.

(F) Graph comparing distribution of microdomain size (in μm^2) as a function of total number of Ca^{2+} events in astrocytes untreated (Control, black trace) or treated with mPTP inhibitors (mPTP-I, red trace). The dotted lines show that in untreated cells microdomains of size 5.5-22 μm^2 contribute to about 50 % of the total number of Ca^{2+} events, and in the cells treated with mPTP-I microdomains with similar size contribute less than 19 % of the total events.

(G) Graph comparing integrated intensity (amplitude x time) as a function of number of Ca^{2+} events in untreated (Control, black trace) and mPTP-I treated (mPTP-I, red trace) astrocytes. The events from membrane-restricted microdomains (5.5-22 μm^2) were analyzed.

(H) Averaged intensity versus time traces of untreated (n =19 cells, left, black trace) and mPTP-I treated (n = 24 cells, right, red trace) astrocytes showing characteristics of Ca^{2+} transients in response to a puff of 100 mM ATP.

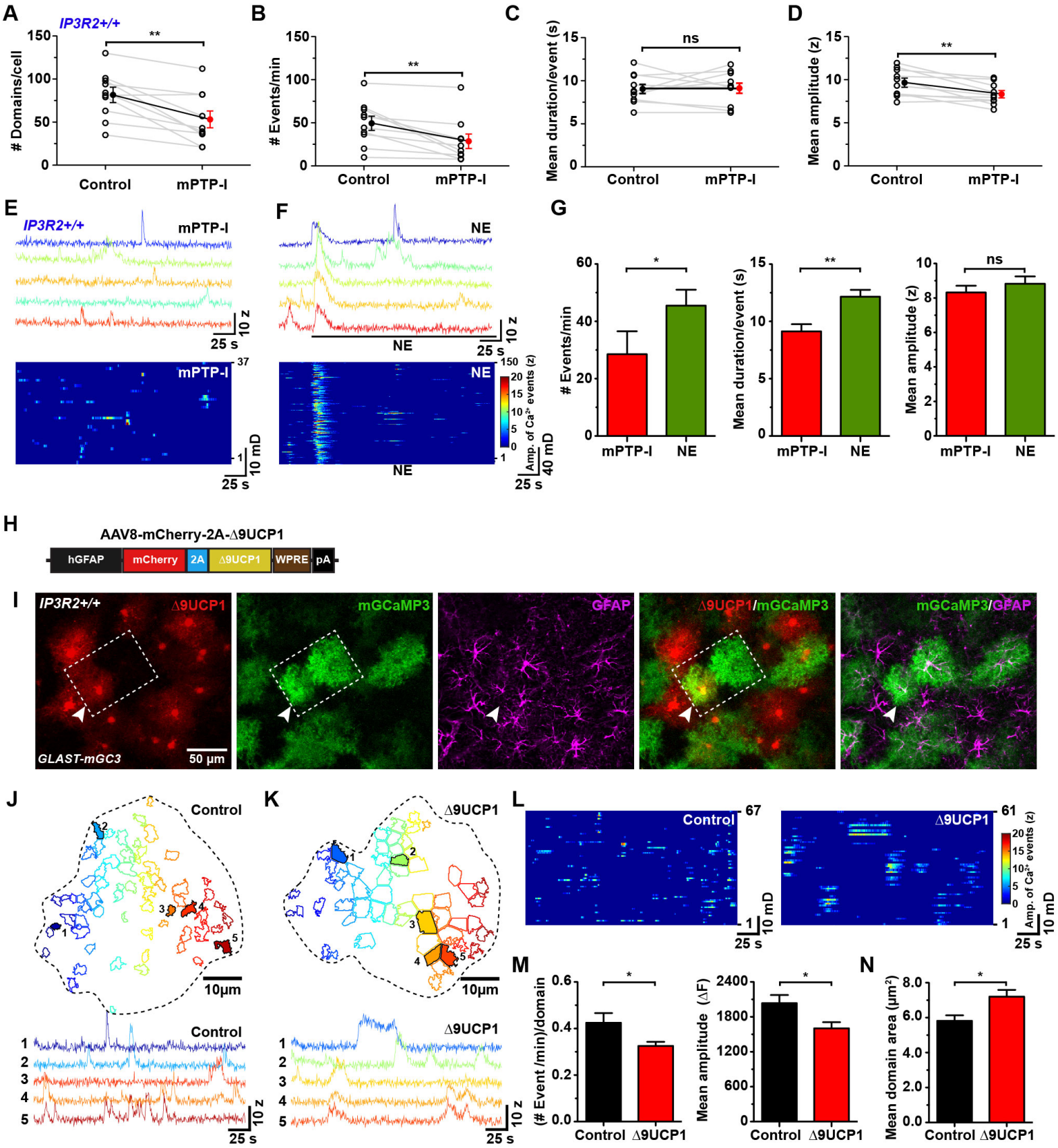

Figure S7, Agarwal et al.

Figure S7: The mitochondrial permeability transition pore (mPTP) regulates spontaneous Ca^{2+} transients in control astrocytes (related to Figure 7)

(A – D) Graphs comparing number of active microdomains/cell (A), frequency of total events (B), duration of events (C) and mean amplitude (D) of microdomain Ca^{2+} transients (z-score) in astrocytes from untreated (Control) and mPTP-I (Cyclosporin A, 20 μM and Rotenone, 10 μM) treated slices derived from *GLAST-mGC3* mice. All experiments performed in 1 μM TTX. Slices were treated with a mPTP-I for 60 min. Data shown as mean ± SEM. N = 10 cells from GLAST-mGC3 mice. ns: not significant, ** $p < 0.005$, * $p < 0.015$, paired two-tailed Student's t-test.

(E) Intensity versus time traces for five microdomains (top) and a raster plot (bottom) displaying timing and intensity of spontaneous Ca^{2+} signals in an astrocyte derived from a cortical brain slice of *GLAST-mGC3* mouse and treated with mPTP-I. All experiments performed in 1 μM TTX.

(F) Intensity versus time traces for five microdomains (top) and a raster plot (bottom) displaying timing and intensity of norepinephrine-induced (NE, 10 μM + mPTP-I) Ca^{2+} signals in an astrocyte treated with mPTP-I from cortical brain slice derived from *GLAST-mGC3* mouse (top). All experiments performed in 1 μM TTX.

(G) Graphs showing the frequency of events/domain (left), mean duration of events (middle) and mean amplitude (right) in mPTP inhibitors (mPTP-I, red) and NE-induced (10 μM, +mPTP-I, green) Ca^{2+} transients from *GLAST-mGC3* mice. All experiments performed in 1 μM TTX. Data shown as mean ± SEM. N = 10 cells for each condition. ns: not significant, * $p = 0.03$, ** $p = 0.006$ paired two-tailed Student's t-test.

(H) Schematic showing a part of the adeno-associated virus serotype 8 (AAV8) vector with a human GFAP promoter fragment (hGFAP, black box), cytosolic mCherry (red box), 2A peptide (cyan box), Δ9 variant of mouse uncoupling protein1 (Δ9UCP1, light brown box), Woodchuck post-transcriptional response element (WPRE, brown box) and SV40 polyA (pA, black box).

(I) Images of cortical astrocytes, from a *GLAST-mGC3* mouse unilaterally injected with *AAV8-mCherry-2A-Δ9UCP1* virus, labeled with anti-mCherry (red), anti-EGFP (green) and ant-GFAP (magenta) antibodies. White dotted box highlights a pair of GFAP+ astrocytes, one expressing both mCherry and mGCaMP3 (arrowhead) and the other expressing mCherry only.

(J) Map of spontaneously active microdomains (top) and intensity versus time traces showing Ca^{2+} transients in five microdomains (bottom) in a control astrocyte (–mCherry; +mGCaMP3). Dashed line highlights cell border and colors correspond to locations of microdomains.

(K) Map of spontaneously active microdomains (top) and intensity versus time traces showing Ca^{2+} transients in five microdomains (bottom) in astrocyte expressing Δ9UCP1 (+mCherry; +mGCaMP3). Dashed line highlights cell border and colors correspond to locations of microdomains.

(L) Raster plot of Ca^{2+} signals from spontaneously active microdomains imaged over a period of 260 s in Control (–mCherry; +mGCaMP3, left) and Δ9UCP1 expressing (+mCherry; +mGCaMP3, right) astrocytes.

(M, N) Histograms comparing frequency of events/domain (left) and mean amplitude (right) (M), and mean domain area (N) in Control (–mCherry; +mGCaMP3, black bars) and Δ9UCP1 expressing (+mCherry; +mGCaMP3, red bars) astrocytes. Data shown as mean ± SEM (n = 12 cells for each condition). * $p < 0.03$, unpaired two-tailed Student's t-test.

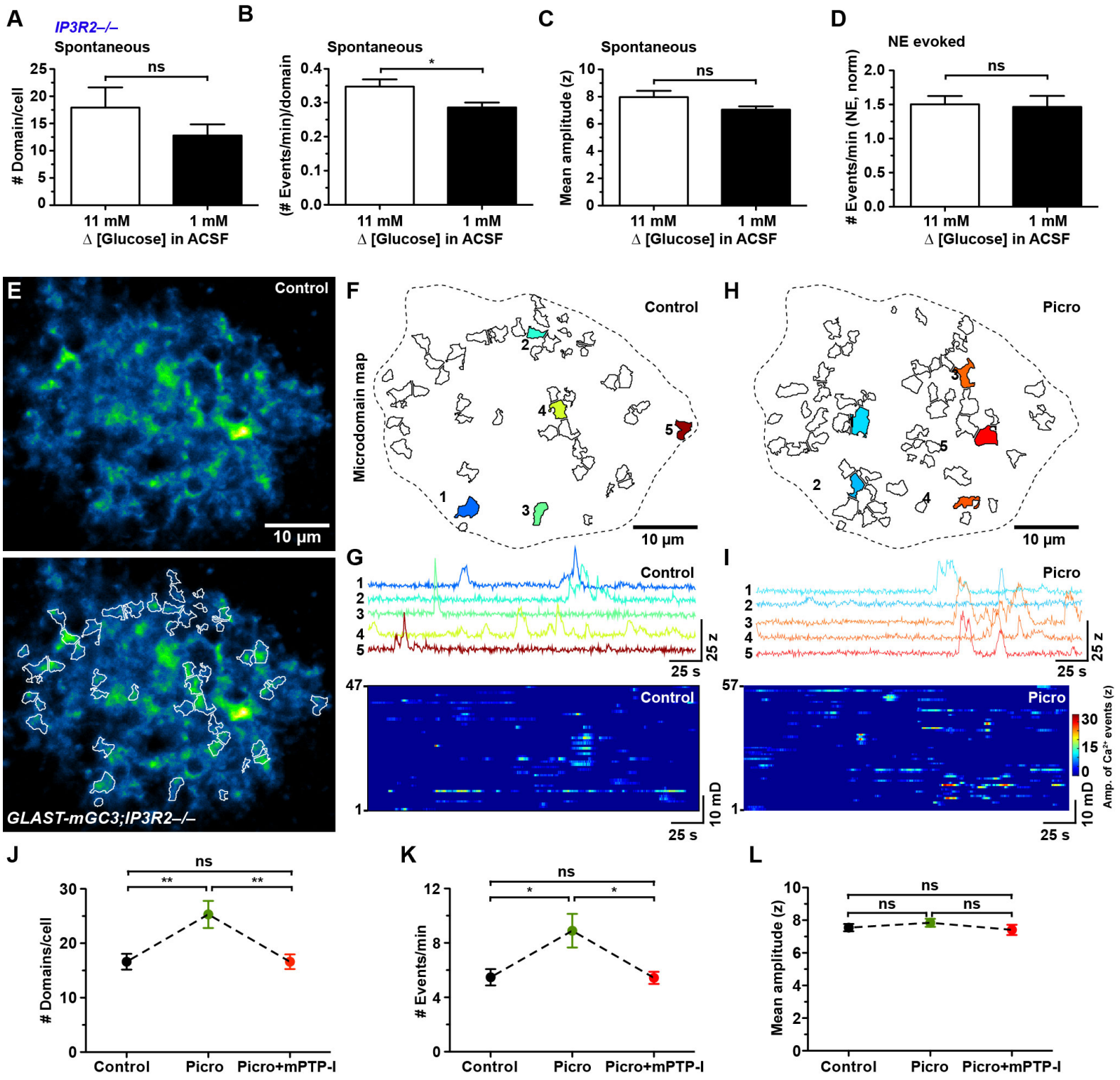

Figure S8, Agarwal et al.

Figure S8: High glucose levels and neuronal activation enhance mPTP activity in astrocytes lacking IP3R2 (related to Figure 8)

(A – C) Histograms comparing number of domains/cell (A), frequency of events/domain (B) and mean amplitude of microdomain Ca^{2+} transients (z-score, C) in regular ACSF (with 11 mM glucose, white bars) and in ACSF containing glucose levels seen *in vivo* (1 mM, black bars). Data shown as mean ± SEM; n = 15 cells, 11 mM glucose; n = 14 cells, 1 mM glucose from *GLAST-mGC3;IP3R2–/–* mice. ns, not significant; * p = 0.038, unpaired two-tailed Student's t-test.

(D) Histograms comparing the frequency (normalized to the baseline frequency) of microdomain events in response to norepinephrine (10 µM, NE) in regular ACSF (with 11 mM glucose, white bars) and in ACSF containing glucose levels seen *in vivo* (1 mM, black bars). Data shown as mean ± SEM (n = 15 cells, 11 mM glucose; n = 14 cells, 1 mM glucose, *GLAST-mGC3;IP3R2–/–* mice). ns, not significant

(E) Image of one astrocyte in an acute brain slice from a *GLAST-mGC3;IP3R2–/–* mouse showing median intensity projection (pseudocolored) of mGCaMP3 fluorescence from 260 s (top). Map of spontaneously active microdomains is overlaid on the median intensity projected image (bottom).

(F) Map showing location of 47 spontaneously active microdomains that occurred during 260 s of imaging. Dashed line highlights cell border.

(G) Intensity versus time traces showing spontaneous Ca^{2+} transients in five microdomains (colors correspond to locations in F) (top). Raster plot of Ca^{2+} signals from 47 spontaneously active microdomains during 260 s (bottom).

(H) Map of 57 spontaneously active microdomains that occurred during 260 s in the presence of picrotoxin (Picro, 100 µM). Dashed line highlights cell border.

(I) Intensity versus time traces showing spontaneous Ca^{2+} transients in five microdomains (colors correspond to locations in H) (top). Raster plot of Ca^{2+} signals from 57 spontaneously active microdomains during 260 s (bottom).

(J – L) Graphs comparing number of domains/cell (J), frequency of events (K) and mean amplitude (K) of microdomain Ca^{2+} transients in control, picrotoxin (Picro, 100 µM), and picrotoxin (100 µM with mPTP-I (Cyclosporin A, 20 µM and Rotenone, 10 µM) (Picro+mPTP-I). Data shown as mean ± SEM (n = 13 cells, *GLAST-mGC3;IP3R2–/–* mice). ns: not significant, ** p <0.001, * p < 0.01 repeated measure one-way ANOVA analysis with Tukey's multiple comparisons post hoc test.

Supplemental Movie Legends

Movie S1: Spontaneous, metabotropic glutamate receptor and noradrenergic receptor agonist evoked Ca^{2+} transients in a control astrocyte, Related to Figure S1

A cortical astrocyte imaged in an acute brain slice from an adult *GLAST-mGC3* mouse. Images were acquired at 2.1 frames/s and displayed at 50 frame/s. Frames 1-600: spontaneous events; Frames 601-1200: events in TTX (1 μM); Frames 1201-1800: events in DHPG (20 μM); Frames 1801-2400: events in norepinephrine (0.5 μM). Agonists experiment were performed in the presence of TTX.

Movie S2: Spontaneous and noradrenergic receptor agonist evoked Ca^{2+} transients in a control astrocyte analyzed by CaSCaDe method, Related to Figure 2 and 3

A cortical astrocyte imaged in an acute brain slice from an adult *GLAST-mGC3* mouse. Images were acquired at 2.1 frames/s, and displayed at 30 frame/s. Frames 1-540: spontaneous events; Frames 541-1080: events in norepinephrine (10 μM). (Left) Pseudo-colored times series images stack and (Right) location of microdomains estimated by CaSCaDe analysis. Experiment was performed in the presence of TTX.

Movie S3: Spontaneous and noradrenergic receptor agonist evoked Ca^{2+} transients in an astrocyte lacking IP3R2, Related to Figure 4

A cortical astrocyte imaged in an acute brain slice from an adult *GLAST-mGC3;IP3R2*$^{-/-}$ mouse. Images were acquired at 2.1 frames/s, and displayed at 30 frame/s. Frames 1-540: spontaneous events; Frames 541-1080: events in norepinephrine (10 μM); (Left) Pseudo-colored times series images stack and (Right) location of microdomains estimated by CaSCaDe analysis. Experiment was performed in the presence of TTX.

Movie S4: Spontaneous and locomotion-induced Ca^{2+} transients in an astrocyte *in vivo*, Related to Figure 5

An astrocyte in primary visual cortex (V1) imaged in an awake adult *GLAST-mGC3* mouse. Images were acquired at 2.1 frames/s, and displayed at 20 frame/s. Frames 1-390: baseline events and Frame 391-490: Treadmill (TM) enforced response. (Left) Pseudo-colored time series image stack and (Right) location of microdomains estimated by CaSCaDe analysis.

Movie S5: Spontaneous and locomotion-induced Ca^{2+} transients in an *IP3R2*$^{-/-}$ astrocyte *in vivo*, Related to Figure 5

An astrocyte in primary visual cortex (V1) imaged in an awake and behaving adult *GLAST-mGC3;IP3R2*$^{-/-}$ mouse. Images were acquired at 2.1 frames/s, and displayed at 20 frame/s. Frames 1-390: baseline events and Frames 391-490: Treadmill (TM) (enforced locomotion) response. (Left) Pseudo-colored time series image stack and (Right) location of microdomains estimated by CaSCaDe analysis.

Movie S6: Simultaneous imaging of mitochondrial dynamics and Ca^{2+} transients, Related to Figure 6

A cortical astrocyte imaged in an acute brain slice from an adult *GLAST-mGC3;mito-EGFP* mouse. Images were acquired at 2.1 frames/s, and displayed at 30 frame/s. Frames 1-540: spontaneous events; Frames 541-1080: events in norepinephrine (10 μM). (Left) Pseudo-colored time series image stack showing mitochondria (red) and Ca^{2+} transients (green). (Right) location of microdomains (green) estimated by CaSCaDe analysis.

Movie S7: Spontaneous Ca^{2+} transients in an astrocyte lacking IP3R2 and treated with mPTP-I, Related to Figure 7

A cortical astrocyte imaged in an acute brain slice from an adult *GLAST-mGC3;IP3R2*$^{-/-}$ mouse, treated with mPTP-I. Images were acquired at 2.1 frames/s, and displayed at 20 frame/s. Frames 1-540: spontaneous events. (Left) Pseudo-colored time series image stack and (right) location of microdomains estimated by CaSCaDe analysis. Experiment was performed in the presence of TTX.

Movie S8: Spontaneous and light-induced Ca^{2+} transients in an astrocyte lacking IP3R2 and treated with mPTP-I, Related to Figure 7

A cortical astrocyte imaged in an acute brain slice treated with mPTP-I, from an adult *GLAST-mGC3;IP3R2*$^{-/-}$ mouse. Images were acquired at 2.1 frames/s, and displayed at 50 frame/s. Frames 1-540: spontaneous events; Frames 541-1080: light-induced events; Frames 1081-1620: events after mPTP-I treatment (following light exposure). (Left) Pseudo-colored time series image stack and (right) location of microdomains estimated by CaSCaDe analysis. Experiment was performed in the presence of TTX.